Tutor/s

Jordi Guilera Sala
*Departament d'Enginyeria química i Química Analítica (UB)*

Elena Martín Morales
*Institut de Recerca en Energia de Catalunya (IREC)*

Grau de Química

# Treball Final de Grau

**Synthesis of $TiO_2$-modified Fischer-Tropsh catalysts by Atomic Layer Deposition**
**Síntesi de catalitzadors de Fischer-Tropsh modificats amb $TiO_2$ mitjançant Atomic Layer Deposition**

Rubén Soler Martín

*June 2024*

Universitat de Barcelona

B:KC Barcelona Knowledge Campus
Campus d'Excel·lència Internacional

Vull agrair als tutors que m'han guiat durant aquest treball: a l'Elena Martín, pel suport que m'ha brindat durant tot el projecte, i al Jordi Guilera, per la dedicació als avenços durant tot aquest temps.

També vull agrair a tothom amb qui he compartit espai de feina a l'IREC, doncs tots ells m'han donat suport i m'han tractat com a un més. Concretament voldria agrair a l'Amine Lwazzani, qui m'ha ensenyat moltíssimes coses. Ha sigut molt gratificant tant a nivell personal com a nivell acadèmic aprendre a l'IREC.

Per acabar, també m'agradaria mencionar a la meva família, que, tant durant aquest treball, com durant tot el grau, han sigut un gran pilar i una inspiració.

# REPORT

# IDENTIFICATION AND REFLECTION ON THE SUSTAINABLE DEVELOPMENT GOALS (SDG)

The Sustainable Development Goals (SDGs), also known as the Global Goals, were adopted by all UN Member States in 2015 as a universal call to end poverty, protect the planet and ensure that all people enjoy peace and prosperity by 2030.TheGoals to which we intend to contribute in this work are:

SDG 7: Affordable and clean energy. To this end, we test whether the small use of $TiO_2$ in FTS helps to improve the productivity of hydrocarbon chains. In addition, the hydrocarbons that are synthesized do not come from petroleum.

SDG 15: protect the life of terrestrial ecosystems. Without the use of petroleum, it can be avoided the deforestation that extraction often causes.

SDG 9: Industry, innovation and infrastructure is also supported in this project, as it contributes to the sustainable development of new technologies.

SDG 13: Climate Action is addressed with the FTS process, which aims to reduce the carbon footprint.

# CONTENTS

# 1. SUMMARY

The Fischer-Tropsch Synthesis (FTS) is a process that forms hydrocarbon chains from CO and $H_2$. In this work, catalysts for the FTS are synthesized. These catalysts consist of an alumina support ($Al_2O_3$), a layer of $TiO_2$ of variable thickness deposited with ALD and Co as active phase. The catalysts synthesized with 5 deposition cycles were found to be significantly more active for FTS than those synthesized with 0, 10 and 20 deposition cycles. Additionally, the selectivity for chains of more than 5 carbons ($C_{5+}$) was very high for all catalysts.

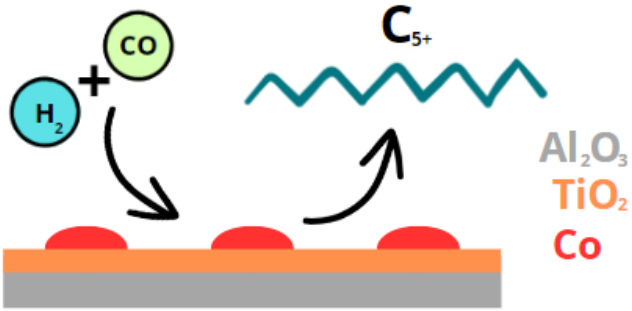


*Scheme of the FTS process with the catalysts synthesized in this work.*

**Keywords:** catalyst, Fischer-Tropsch, hydrocarbon, ALD.

# 2. RESUM

La Síntesi de Fischer-Tropsch (FTS) és un procés que forma cadenes d'hidrocarburs a partir de CO i $H_2$. En aquest treball, se sintetitzen catalitzadors per a FTS. Aquests catalitzadors consisteixen en un suport d'alúmina ($Al_2O_3$), una capa de $TiO_2$ de gruix variable depositada amb ALD i Co com fase activa. Els catalitzadors sintetitzats amb 5 cicles de deposició van resultar ser més actius per a FTS que els sintetitzats amb 0,10 i 20 cicles de deposició. Adicionalment, la selectivitat per a les cadenes de més de 5 carbonis ($C_{5+}$) va ser molt alta per a tots els catalitzadors.

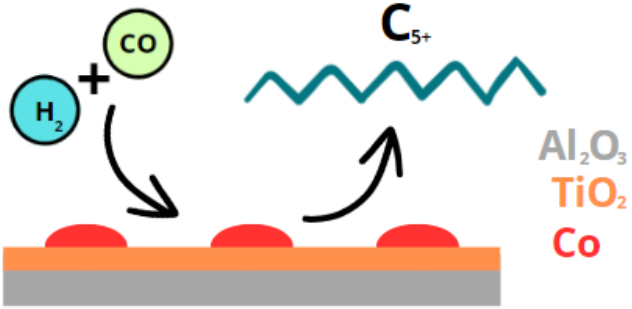


*Esquema del procés FTS amb els catalitzadors sintetitzats en aquest treball.*

**Paraules clau**: catalitzador, Fischer-Tropsch, hidrocarburs, ALD.

# 3. INTRODUCTION

## 3.1. ATOMIC LAYER DEPOSITION

Atomic Layer Deposition (ALD) is a technique that allows for the controlled deposition of metallic oxide, nitride, sulfide, and metal films onto substrates of different natures, with highly precise and uniform characteristics.[1] ALD ensures highly precise control over thickness and composition of the deposited films, resulting in uniform surfaces, atomic-level thickness control, and reproducibility ALD deposition processes are cyclic and self-limiting, stopping once the layer is completely covered to prevent excessive material deposition. [1]

The mechanism of deposition by ALD, illustrated in Figure 1, proceeds as follows. Initially, a pulse of the first precursor, usually an organometallic compound with high vapor pressure (such as trimethylaluminium (TMA), diethylzinc (DEZ), or titanium tetrachloride) [2], is introduced and reacts with the active sites of the substrate, partially binding its ligands. After this semireaction with the support, a purge step follows to remove the ligands, other byproducts and the unreacted precursor. Next, a pulse of a second precursor is introduced, usually an oxidizer or reducer (for example $O_3$, $O_2$, $H_2$ or $H_2O$) [3], which reacts with the components bound to the substrate. At this point, the reaction is completed, the precursor ligands are removed and the

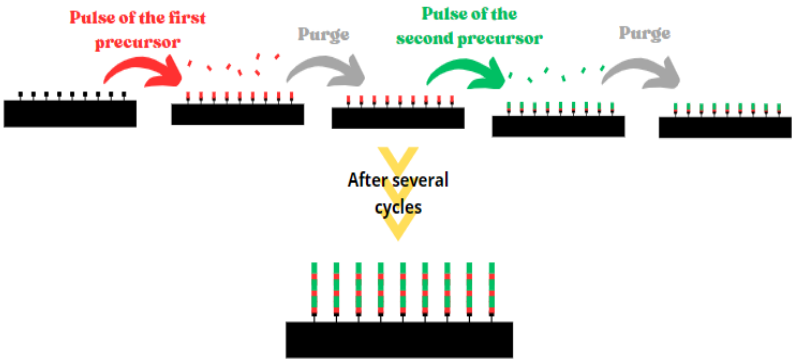


*Figure 1. Scheme of the ALD mechanism.*

active sites of the support are regenerated. Another purge step is then performed to remove the byproducts of this semireaction. [1]

The reaction conditions, such as reactants, temperature, or number of cycles, determine the thickness of the deposited film. Typically, higher temperatures and more cycles (or deposition times) result in thicker films. [4]

The concept of ALD emerged around the 1970s, with the main goal of depositing thin films on electroluminescent flat panel displays. It gained renewed attention in the 1990s, particularly for silicon-based microelectronics. Since the 2000s, it has been used in microelectronics, photovoltaics, sensors, battery cells, and other important applications such as catalysis. [1],[5]

One of the deposition techniques most frequently compared to ALD is Chemical Vapor Deposition (CVD), as they use a similar technical principle (pulse emission). However, in CVD, the reactant pulses are emitted simultaneously, which gives ALD better control over the layer growth. Additionally, as CVD operates at higher temperatures, ALD becomes a more adequate technique to avoid decomposition of part of the sample or unwanted reactions.

Other well-known techniques include pulsed layer deposition (PLD), a process in which a laser is used to vaporize the target, Molecular beam epitaxy (MBE), a physical deposition method that forms layers to achieve well-defined crystalline structures or Sputtering, a technique based on ion bombardment of a target. Table 1 shows how ALD stands out in many characteristics compared to various similar techniques. Therefore, ALD is established as a good technique in all aspects, with a low deposition rate that can be easily addressed by increasing the number of ALD cycles. This not only compensates for the poor deposition rate but also ensures exceptional control over layer thickness.[6]

*Table 1. Comparison between some deposition techniques. [3]*

| | PLD | Sputtering | MBE | CVD | ALD |
|---|---|---|---|---|---|
| **Low substrate temperature** | Good | Good | Good | Varies | Good |
| **Deposition rate** | Good | Good | Fair | Good | Poor |
| **Film density** | Good | Good | Good | Good | Good |
| **Thickness** | Fair | Good | Fair | Good | Good |

In addition to the techniques mentioned, one of the most commonly used methods for depositing small quantities of material is incipient wetness impregnation (IWI). This method involves impregnating a support with a solution of salts, usually nitrates, followed by drying and

subsequent treatment, typically through calcination and/or reduction. The primary difference between ALD and IWI, apart from the technical simplicity and low cost of IWI, is that ALD offers much higher control over the deposition process, allowing for higher active phase dispersions and, therefore, reduced and optimized use of critical materials. [7]

## 3.2. SYNTHESIS OF $TiO_2$-BASED CATALYSTS BY ALD

In the field of catalysis, ALD has shown considerable potential for synthesizing high-specific-surface-area catalytic materials. The technique offers unique advantages in the preparation of heterogeneous catalysts, allowing uniform dispersion of active materials on porous supports and precise modification of active sites at the molecular level. This has been demonstrated in recent studies where ALD has been used to deposit precious metals and metal oxides on various supports, resulting in catalysts with enhanced activities and selectivities for specific reactions. [3]

$TiO_2$ catalysts are increasingly attracting interest due to their unique properties and versatility in various chemical reactions and photochemical processes. Interesting properties of $TiO_2$ are the conductivity provided by oxygen vacancies in its structure, as well as being highly corrosion resistant, which make it a good material for catalytic applications, either as active phase, promoter or support.. [9],[10]

Some of the most common $TiO_2$ precursors for ALD are $TiCl_4$ (Titanium tetrachloride), $Ti(NMe_2)_4$ (TDMAT or Tetrakis(dimethylamino)titanium(IV)), or $Ti(NEt_2)_4$ (TDEAT or Tetrakis(diethylamino)titanium(IV)). [11]

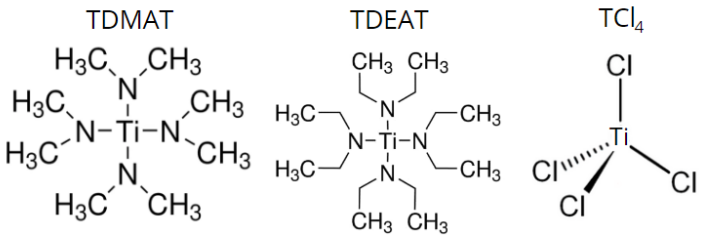


*Figure 2. TDMAT, TDEAT and $TiCl_4$ structures.*

During $TiO_2$ deposition, when the precursor pulse (in this case TDMAT, as used in this work) is emitted, the (-OH) groups on the surface react with the organometallic, causing it to lose ligands in the process:

$$2(\text{-OH}) + Ti[N(CH_3)_2]_4 \rightarrow (O_2Ti[N(CH_3)_2]_2^* + 2(HN(CH_3)_2) \quad \text{[Eq. 1]}$$

In the second part of the reaction, the oxidant (water in this case) fully oxidizes the organometallic:

$$Ti[N(CH_3)_2]_2^* + 2H_2O \rightarrow Ti(OH)_2^* + 2HN(CH_3)_2 \quad \text{[Eq. 2]}$$

The * symbol indicates a surface adsorption site, representing where the compound binds to the substrate surface. In this sense, $Ti(OH)_2$ is bound to the oxygen atoms that were previously part of the support surface [12].

An important application of $TiO_2$ deposition is photoelectrochemical (PEC) water splitting. For example, the activity of a catalyst based on fluorine-doped tin oxide (FTO) was improved with a layer of $TiO_2$, deposited using TDMAT[9] . $TiO_2$ conferred enhanced conductivity provided by oxygen vacancies in its structure and higher corrosion resistance.

Another example of $TiO_2$ use in catalysis is the glycerol oxidation reaction. For this reaction, a commercial Au/C support was coated using 30 ALD cycles with $TiCl_4$ as the titanium precursor and water as the oxidant, followed by thermal treatment at 400ºC for 1 hour in a $N_2$ atmosphere. Interactions between Au and $TiO_2$, facilitated by ALD-formed Au-Ti interfaces, enhanced catalytic activity and stability during the electrooxidation reaction.[13]

Activity enhancement is also observed when ALD is used to deposit $TiO_2$ for phenol hydrogenation, an important process for the production of Nylon 6 and Nylon 66. In this case an interaction is formed between Pt and $TiO_2$ in which Pt is embedded within the $TiO_2$ layer, which increases the reactivity.[14]

As can be seen, the use of ALD technology to deposit $TiO_2$ has promising applications, such as increased corrosion stability, increased catalyst conductivity and increased catalyst activity due to the interaction between $TiO_2$ and the active metal.

## 3.3. FISCHER-TROPSCH SYNTHESIS

The Fischer-Tropsch Synthesis (FTS) is a chemical process to produce hydrocarbon chains of variable length from the reaction of a mixture of $H_2$ and CO, known as syngas.[11],[15],[16]

FTS comprises a set of reactions that can be expressed by two equations, depending on whether saturated or unsaturated chains are formed [16]:

$(2n+1)\ H_2 + n\ CO \rightarrow C_nH_{2n+2} + n\ H_2O$ [Eq. 3]

$2n\ H_2 + n\ CO \rightarrow C_nH_{2n} + n\ H_2O$ [Eq. 4].

The FTS reaction process is as follows: first, the reactants diffuse and enter the pores. This way, they approach the active sites of the catalyst (generally the metal impregnated on the surface). Then, they adsorb onto these active sites. Next, the chain initiation occurs, followed by chain growth and then chain termination. After this, the product desorbs and exits the pore of the catalyst. [17]

The synthesis of certain hydrocarbons becauses of particular interest because they serve as the source for important fuels, specifically Sustainable Aviation Fuel (SAF). This term refers to fuels meeting specific sustainability criteria [12]. In fact, considering that in 2019, according to the International Air Transport Association (IATA), the global aviation industry transported over 4.5 billion air travelers, accounting for approximately 2% of anthropogenic greenhouse gas (GHG) emissions, SAF represents a significant ally in reducing $CO_2$ emissions [18].

Despite the significant economic and environmental interest in FTS, it presents a challenge in terms of selectivity, as controlling the length of the hydrocarbon chains formed is difficult.

The factors that affect the selectivity, are mainly divided into two different groups:

- Engineering factors, such as reaction conditions and reactor design.
- Catalytic factors, such as the material of the catalyst support, the type of pores it has, the nature of the active phase, the oxidation state of the active phase, or the use of dopants, among others. [17],[19].

For example, it has been observed that as the active surface area of the catalysts increases, their activity also increases, which is why porous supports are used. [16] Additionally, it has been demonstrated that catalysts with Co as active phase can increase the chain length of the hydrocarbons formed, thereby enhancing the efficiency of the reaction for clean and environmentally friendly fuel production.[15]

Considering the socio-economic importance of aviation fuels and the criticality of investing in technology that reduces the carbon footprint, research into improving the reactivity and selectivity of FTS catalysts is a promising field of study for the well-being of society.

# 4. OBJECTIVES

This work is orientated in obtaining suitable avion fuel (SAF) using Fischer-Tropsch Synthesis (FTS). In this procedure a mix of CO and $H_2$ (syngas) react to form hydrocarbon chains of variable length.

The main goal of this work is develop catalysts to optimize the FTS, depositing films of $TiO_2$ with variable growth on conventional $Al_2O_3$ supports by Atomic Layer Deposition (ALD).

Evaluation of catalytic tests will be performed to measure the selectivities and conversions of the catalysts, focusing on the effect of the $TiO_2$ deposition in the catalysts.

# 5. EXPERIMENTAL SECTION

## 5.1. MATERIALS

The reagents used in the work are shown in Table 2.

*Table 2. Reagents used in this work.*

| Reagents |
|---|
| Tetrakis(dimethylamino)titanium(IV) (TDMAT (99.99%-Ti), PURATREM) |
| Nitrate hexahydrate ($Co(NO_3)\cdot 6H_2O$, ≥ 98%, Merk) |
| γ-$Al_2O_3$, 500 µm spheres, Norpro Saint-Gobain |
| Syngas (33.13% CO; 66.7 % $H_2$, Linde) |
| $H_2$, (>99,9999%, Linde) |

## 5.2. $TiO_2$ DEPOSITION

The ALD reactor (PICOSUN™ ALD system), represented in Figure 3, was used for the deposition of $TiO_2$. The reaction was carried out by emitting TDMAT and water pulses. An ALD cycles consist of ten TDMAT pulses of 0.2 s each followed by a purge of 1,0 s (the last one being longer, 300.0 s) and ten pulses of water pulses of 0.1 s followed by a purge of 1.0 s (the last one being longer, 300.0 s), see Figure 4. The reactor chamber was at 150 ºC, while the w ater was at room temperature and TDMAT was at 70 ºC.

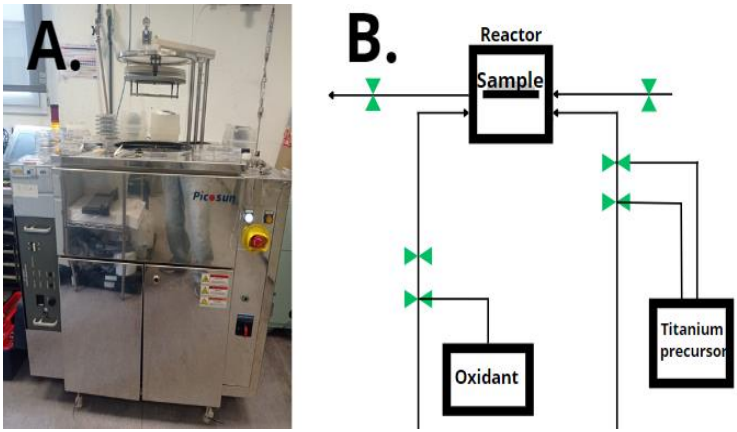


*Figure 3. (A) Photograph of the ALD reactor. (B) Scheme of the ALD reactor.*

Three different types of supports were synthesized with ALD deposition, differing in the number of deposition cycles. These supports are named with the following nomenclature: $TiO_2$(nc)/$Al_2O_3$, being n the number of cycles applied (5, 10, and 20), see Figure 5.

### 5.3 COBALT IMPREGNATION

The cobalt catalysts were synthesized by wet impregnation method to have 17.5% Co loading.

*Figure 5. Scheme of supports prepared in this work.*

1.5 g of support were impregnated with 1.6 g of $Co(NO_3)_2 \cdot 6H_2O$ dissolved in 4mL of water. The samples were dried in a rotary evaporator under vacuum at 80ºC and rotation.

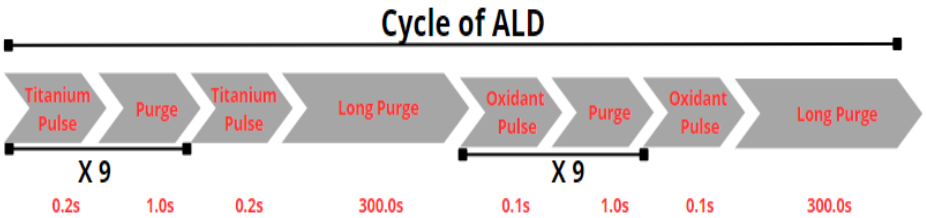


*Figure 4. Scheme of an ALD cycle.*

When the supports were impregnated, they were calcined. The temperature was increased

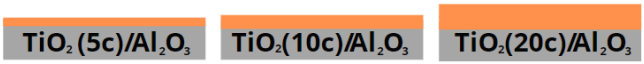


by 5ºC/min until it reached 100ºC. This temperature was maintained for 12h and increased to 275ºC with a ramp of 1ºC/min.

The nomenclature after the formation of cobalt oxide on the surface is Co/$TiO_2$(nc)/$Al_2O_3$. Additionally, a reference catalyst was synthetized on bare $Al_2O_3$ support, following the same impregnation procedure and is referred to as Co/$Al_2O_3$, see Figure 6.

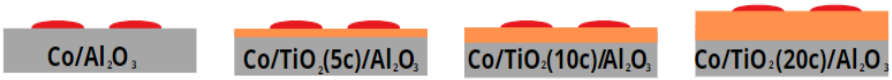


*Figure 6. Scheme of Co-based catalysts prepared in this work.*

After calcination, in-situ reduction of the catalyst was performed in the reactor to obtain metallic cobalt.

A leak test was carried out prior to the reduction. The reduction conditions were: 2 hours at 120°C with a flow of $H_2$ at 45.8 normal·mL/min, to remove any remaining ceres accumulated in the ducts reactor. After cleaning, the temperature was raised with a ramp of 0.5°C/min up to 380°C, maintaining the same flow for 11 hours. Then, it was allowed to cool down with a flow of 22.3 normal·mL/min until reaching 160°C.

## 5.4 FISCHER-TROPSCH CATALYTIC TESTS

The catalytic FTS tests were conducted in a fixed-bed reactor (Microactivity, PID Eng&Tech). A reactor setup in series was employed, as represented in Figure 7.

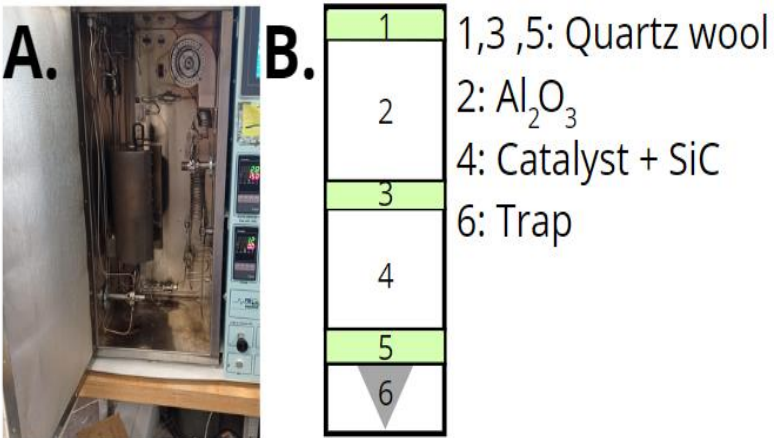


*Figure 7. (A) Photograph of Microactivity reactor. (B) Reactor scheme.*

$Al_2O_3$ is used to improve heat distribution in the system. SiC was used to prevent hot spots and a trap made of porous ceramic material to prevent wax accumulation in the reactor.

FTS was carried out at 230ºC and 20 bar. The flow rates were adjusted depending on the CO conversion obtained to ensure comparability.

## 5.5 CHARACTERIZATION

Characterization of the supports and the catalysts was conducted before the reduction reaction.

The densities of the four supports were measured on the Quantachrome Micro Ultrapyc 1200e Automatic Gas Pycnometer. In the process, helium at 20psig pressure was used for the samples. Adsorption/desorption isotherms of the catalysts and supports were measured using $N_2$-physisorption in a TriStar II 3020-Micrometrics sorption analyzer.

The catalysts composition was measured by inductively coupled plasma (ICP) on an Optima Perkin Elmer 3200 RL. To measure which crystalline structures were found on the surface, the X-ray diffraction (XRD) technique was used. For this purpose, a Burker XRD D8 Advance A25 diffractometer was used. Furthermore, the particle size could be calculated using the Scherrer equation: $\mathrm{D} = \frac{\kappa\lambda}{\beta cos\theta}$ [Eq. 8]. [20]

Temperature programmed reduction ($H_2$-TPR) was made on an Autochem 2890 (Micrometrics) with 50NmL/min of $H_2$ flow (12% $H_2$/Ar). This is a technique that measures the temperatures to which samples are reduced in the presence of $H_2$. CO-Chemisorption tests were performed to determine the active metal surface area and metal dispersion of the catalysts on an Autochem 2890 (Micrometrics). The samples were reduced at 380ºC make the measurements.

# 6. RESULTS AND DISCUSSION

## 6.1 MATERIAL CHARACTERIZATION

The skeletal densities of the supports are presented in Table 3. The tabulated density of $TiO_2$ is slightly higher (4.17 g/cm$^3$) [21] than that of alumina (3.99 g/cm$^3$) [22]. The similar densities of $Al_2O_3$ and $TiO_2$ makes no major differences aparent. Despite this, it is noted that and as the amount of $TiO_2$ deposited increases, the density increases minimally, except for the Co/$TiO_2$(10c)/$Al_2O_3$ sample, which shows anomalous behavior.

*Table 3. Supports density measurements .*

| | $Al_2O_3$ | $TiO_2$(5c) /$Al_2O_3$ | $TiO_2$(10c) /$Al_2O_3$ | $TiO_2$(20c) /$Al_2O_3$ |
|---|---|---|---|---|
| **Medium density (g/cm3)** | 3.196 ± 0.004 | 3.234 ± 0.003 | 3.136 ± 0.002 | 3.318 ± 0.004 |

Figure 8 displays the $N_2$ adsorption/desorption isotherms of the supports are shown. The isotherms have similar typical shape of mesoporous materials [23] and the $TiO_2$(5c)/$Al_2O_3$ support can adsorb more than its homologs, although it is closely followed by the support without deposition. Although it was expected that $TiO_2$ saturating the surface would reduce the surface area of the support, it can be explained that the $TiO_2$(5c)/$Al_2O_3$ support adsorbs slightly more because it has few depositions and $TiO_2$ has many vacancies. Increasing the number of ALD cycles results in a decrease in the surface area of the supports, as observed in samples $TiO_2$(10c)/$Al_2O_3$ and $TiO_2$(20c)/$Al_2O_3$.

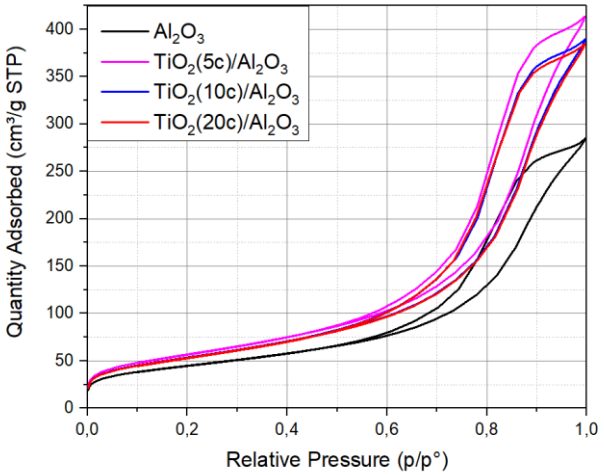


*Figure 8. Supports BET isotherms.*

Table 4 confirms the results; the support with the highest surface area is $TiO_2(5c)/Al_2O_3$. This observation aligns with the trend indicated by the isotherms. $N_2$-physisorption was also performed after cobalt impregnation. The forms of their isotherms are similar (Figure 9), and as can be seen in the figure and in table 4, the expected trend is followed: the higher the number of deposition cycles, the less adsorption. Comparing the BET Surface Area ($SA_{BET}$) of supports and catalysts, it is clear that the presence of Co decreases the adsorption of $N_2$, since the oxide covers the surface.

*Table 4. Supports and catalysts BET Surface Area.*

| Supports | ($SA_{BET}$) ($m^2/g$) | Catalysts | ($SA_{BET}$) ($m^2/g$) |
|---|---|---|---|
| $Al_2O_3$ | *202.05* | *$Co/Al_2O_3$* | *161.78* |
| $TiO_2(5c)/Al_2O_3$ | *205.30* | *$Co/TiO_2(5c)/Al_2O_3$* | *161.97* |
| $TiO_2(10c)/Al_2O_3$ | *193.76* | *$Co/TiO_2(10c)/Al_2O_3$* | *155.33* |
| $TiO_2(20c)/Al_2O_3$ | *192.6* | *$Co/TiO_2(20c)/Al_2O_3$* | *155.74* |

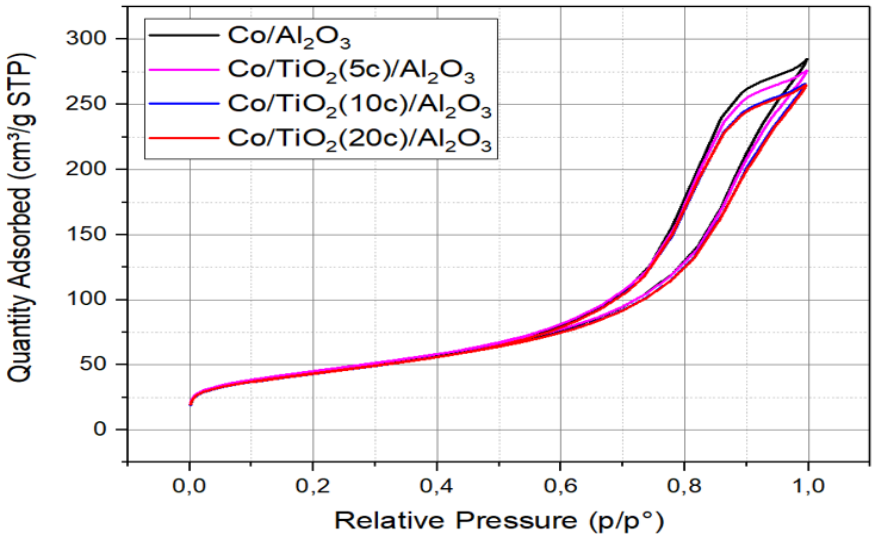


*Figure 9. Catalysts BET isotherms.*

*Table 5. Co and Ti quantities (wt. %)in catalysts (Indicative lower límit: 0.50% for Co and 0.25% for Ti).*

| Catalyst | % Co | % Ti |
|---|---|---|
| Co/ $TiO_2$(5c)/$Al_2O_3$ | 14.66 | 0.36 |
| Co/ $TiO_2$(10c)/$Al_2O_3$ | 15.22 | 0.65 |
| Co/ $TiO_2$(20c)/$Al_2O_3$ | 14.93 | 1.21 |

The ICP results of the $TiO_2$-modified catalysts show the correlation between ALD cycles and the quantity of Ti in the catalysts, see Table 5. The more ALD cycles deposited correlate with the higher amounts of titanium in the sample, confirming the accuracy of the depositions. In fact, a linear trend is shown between the number of stools and the amount of Ti in the sample. The quantities of Co in the catalysts are similar (around 15%) and close to the theoretical 17.5% Co loading.

The XRD characterization (Figure 10) shows different crystalline substances in the four synthesized catalysts. The analysis of the catalysts is very similar, except in the case of $Co/Al_2O_3$ as there are no peaks matching Ti-containing substances. Furthermore, it can be seen that although all catalysts contain Co species, namely $Co_3O_4$ and $Co(OH)_2$, the $Co/Al_2O_3$ catalyst lacks peaks, indicating the presence of $Co(OH)_2$ is favored by the $TiO_2$ promoter.

The average particle sizes of $Co_3O_4$ (10-14 nm) and $Co(OH)_2$ (32-25 nm) were estimated and no major differences were observed between the different catalysts.

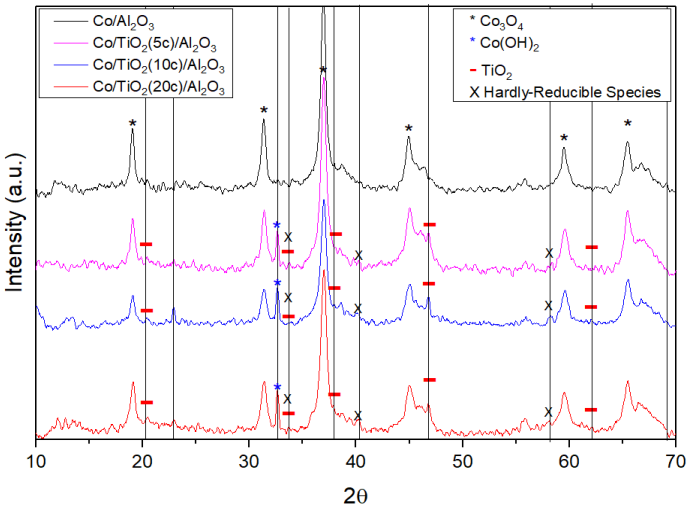


*Figure 10. XRD diffractograms of the Co-based catalysts.*

The $H_2$-TPR profiles of the catalysts (Figure 11) show three distinct reduction processes. The first one, is attributed to the reduction of $Co_3O_4$ into to CoO, at temperatures close to 200ºC. There is also a peak around 300ºC, marked with a dashed line, indicative of the reduction of CoO to metallic Co. Finally, the reduction process that takes place at temperatures higher than 400ºC (higher than 600ºC in the case of $Co/Al_2O_3$) is attributed to the reduction of cobalt aluminates and other hardly reducible species. The reductions of the cobalt oxides and the hardly reducible species are favored in the $TiO_2$-containing catalysts at lower temperatures.

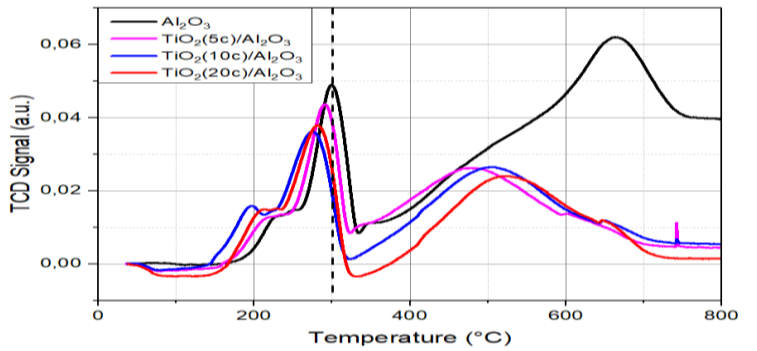


*Figure 11. $H_2$-TPR profil·les of Co-based catalysts.*

The a ctive metal surface area and metal dispersion of the Co-based catalysts was estimated by CO-chemisoprtion. As displayed in Table 6, the $Co/Al_2O_3$ catalyst as a higher active metal surface area and metal dispersion It can be explained by the fact that it does not contain $TiO_2$ which interferes with Co. What is more remarkable is that $Co/TiO_2$ (5c)/$Al_2O_3$ and $Co/TiO_2$ (20c)/$Al_2O_3$ have similar values, while $Co/TiO_2$ (10c)/$Al_2O_3$ break the trend again.

*Table 6. Active Metal Surface Area and Metal Dispresion of catalyst*

| Catalyst | Active Metal Surface Area ($m^2$/g sample) | Metal Dispersion (%) |
|---|---|---|
| $Co/Al_2O_3$ | 1,48 | 1,53 |
| $Co/TiO_2(5c)/Al_2O_3$ | 0,77 | 0,65 |
| $Co/TiO_2(10c)/Al_2O_3$ | 0,41 | 0,35 |
| $Co/TiO_2(20c)/Al_2O_3$ | 0,73 | 0,61 |

## 6.2 CATALYTIC ACTIVITY IN FISCHER-TROPSCH

Figure 12 shows the CO conversion in the FTS tests with each of the catalysts. It can be seen that the conversion is significantly higher for $Co/TiO_2(5c)/Al_2O_3$ than for the other catalysts for all the syngas fluxes applied. It can be observed that the conversion decreases as the flow rate increases. This happens because the higher the flow rate, the less time the reactants have to form hydrocarbon chains, therefore less CO and $H_2$ will have reacted. The conversion trends show that the $Co/Al_2O_3$ catalyst exhibits the second highest CO conversions, but closely followed by $Co/TiO_2(10c)/Al_2O_3$ and $Co/TiO_2(20c)/Al_2O_3$, respectively. The $Co/Al_2O_3$ catalyst presents higher Active Metal Surface Area, as pointed by the CO-chemisorption results, which explains the highest activity of this material is that the active centres have not been saturated by the Co.

Based on t he article by Melaet et al., 2014, it can be theorised that in our system the reduction reaction of $Co_3O_4$ to CoO is partially produced and partially the encapsulation, i.e. $TiO_2$ envelops Co particles, since in the mentioned article it is said that at 250ºC CoO is formed but that at 450ºC encapsulation occurs. In our case, the reduction to CoO occurs around 200ºC, but we do notice a signal in the $H_2$-TPR around 450ºC (Figure 11), which could be attributable to the encapsulation mentioned above. This would explain the high conversion of CO in the tests with the $Co/TiO_2(5c)/Al_2O_3$ catalyst (because it is mentioned that CoO is more active than Co),

but it also explains why in the presence of more $TiO_2$ the conversions decrease, as more encapsulation is formed due to the larger quantities available.

Although we reached 380ºC during the reduction (insufficient compared to 450ºC in the article), it should be noted that the pressure conditions are not the same. [24]

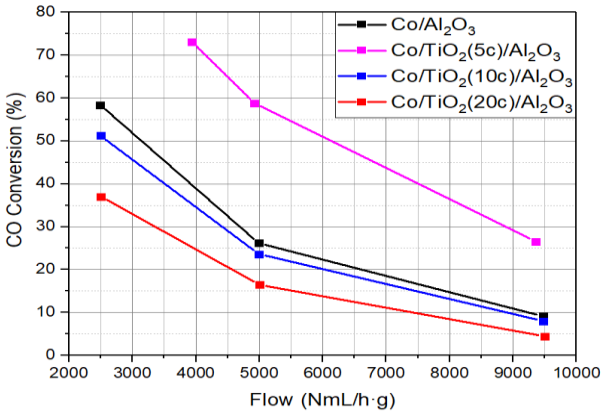


*Figure 12. Flow vs CO conversion.*

Table 9 shows the selectivity data at $C_{5+}$. It can be seen that all catalysts have very similar selectivities in all fluxes, indicating that the presence of $TiO_2$ does not have a significant effect on the length of the hydrocarbon chains formed with FTS.

It is observed that the yields in the $Co/TiO_2(5c)/Al_2O_3$ catalyst are much higher than those observed ofr the rest of catalysts tested. Specifically, if flows close to 5000 (NmL h−1 g−1) are compared, it can be seen that the yield of this catalyst exceeds by approximately double that of both $Co/Al_2O_3$ and $Co/TiO_2(10c)/Al_2O_3$. The $Co/TiO_2(20c)/Al_2O_3$ catalyst presented the worst yields.

*Table 9. Selectivities at $C_{5+}$, CO conversions and yields for all fluxes and catalysts.*

| Catalyst | Flux (NmL h−1 g−1) | Selectivity $C_{5+}$ (%) | X CO (%) | Yield (%) |
|---|---|---|---|---|
| $Co/Al_2O_3$ | 9474,73 | 88,6 | 9,12 | 8,08 |
| | 4986,7 | 92,2 | 26,20 | 24,16 |
| | 2493,35 | 92,2 | 58,36 | 53,80 |
| $Co/TiO_2(5c)/Al_2O_3$ | 9356,53 | 86,2 | 26,58 | 22,91 |
| | 4924,49 | 92,2 | 58,77 | 54,19 |
| | 3939,59 | 90,2 | 73,04 | 65,88 |
| $Co/TiO_2(10c)/Al_2O_3$ | 9479,46 | 89,59 | 8,02 | 7,18 |
| | 4989,19 | 94,29 | 23,64 | 22,29 |
| | 2494,6 | 93,32 | 51,18 | 47,76 |
| $Co/TiO_2(20c)/Al_2O_3$ | 9504,75 | 87,97 | 4,45 | 3,91 |
| | 5002,5 | 93,54 | 16,46 | 15,39 |
| | 2501,25 | 95,8 | 37,03 | 35,48 |

# 7. CONCLUSIONS

Considering that the quantities of Ti and Co in the catalysts on which it were measured, it can be concluded that the Co impregnation have been done satisfactorily and that the number of deposition cycles is directly proportional to the amount of $TiO_2$ deposited on the sample. This affirmation is also supported by the fact that the BET Surface Area decreases with the addition of $TiO_2$, as it shows that the pores of the $Al_2O_3$ support are covered by the oxide, except for the $Co/TiO_2(5c)/Al_2O_3$ catalyst, which can be explained by the low presence of Ti.

The $Co/TiO_2(5c)/Al_2O_3$ catalyst shows much higher CO conversions than the rest. This indicates that under the conditions in which the experiments were carried out, low Ti%, is close to 0.36%, favour the activity of the catalyst in the FTS process.

Considering that the selectivities at $C_{5+}$ are high, it can be determined that the synthesized catalyst is highly effective for SAF production, as many of the resulting hydrocarbons are suitable for use as fuels. This represents an interesting field for the development of green energy since, particularly through the FTS process This, together with the small amount of Ti required, provides us with a very promising avenue for the development of fuels.

# 8. REFERENCES AND NOTES


[1] Oneill BJ, Jackson DHK, Lee J, Canlas C, Stair PC, Marshall CL, et al. Catalyst design with atomic layer deposition. ACS Catal 2015;5:1804–25. https://doi.org/10.1021/cs501862h.

[2] Tan K, Jensen S, Feng L, Wang H, Yuan S, Ferreri M, et al. Reactivity of Atomic Layer Deposition Precursors with OH/H2O-Containing Metal Organic Framework Materials. Chemistry of Materials 2019;31:2286–95. https://doi.org/10.1021/acs.chemmater.8b01844.

[3] Clary JM, Van Norman SA, Funke HH, Su D, Musgrave CB, Weimer AW. Highly dispersed Co deposited on Al2O3 particles via CoCp2 + H2 ALD. Nanotechnology 2020;31:175703–175703. https://doi.org/10.1088/1361-6528/ab68e1.

[4] Cop P, Celik E, Hess K, Moryson Y, Klement P, Elm MT, et al. Atomic Layer Deposition of Nanometer-Sized CeO2 Layers in Ordered Mesoporous ZrO2 Films and Their Impact on the Ionic/Electronic Conductivity. ACS Appl Nano Mater 2020;3:10757–66. https://doi.org/10.1021/acsanm.0c02060.

[5] Filez M, Dendooven J, Detavernier C. Catalysts made from vapour. Nat Catal 2024;7:2–3. https://doi.org/10.1038/s41929-023-01098-w.

[6] Oke JA, Jen TC. Atomic layer deposition and other thin film deposition techniques: From principles to film properties. Journal of Materials Research and Technology 2022;21:2481–514. https://doi.org/10.1016/j.jmrt.2022.10.064.

[7] Sietsma JRA, Jos van Dillen A, de Jongh PE, de Jong KP. Application of ordered mesoporous materials as model supports to study catalyst preparation by impregnation and drying. Stud Surf Sci Catal 2006;162:95–102. https://doi.org/10.1016/S0167-2991(06)80895-5.

[8] Ramachandran RK, Detavernier C, Dendooven J. 4 Atomic Layer Deposition for Catalysis. n.d.

[9] Moehl T, Suh J, Sévery L, Wick-Joliat R, Tilley SD. Investigation of (Leaky) ALD TiO2 Protection Layers for Water-Splitting Photoelectrodes. ACS Appl Mater Interfaces 2017;9:43614–22. https://doi.org/10.1021/acsami.7b12564.

[10] Dey S, Mehta NS. Synthesis and applications of titanium oxide catalysts for lower temperature CO oxidation. Current Research in Green and Sustainable Chemistry 2020;3:100022. https://doi.org/10.1016/j.crgsc.2020.100022.

[11] Niemelä J-P, Marin G, Karppinen M. Titanium dioxide thin films by atomic layer deposition: a review. Semicond Sci Technol 2017;32:93005. https://doi.org/10.1088/1361-6641/aa78ce.

[12] Promjun T, Rattana T, Pansila PP. Kinetic study on initial surface reaction of titanium dioxide growth using tetrakis(dimethylamino)titanium and water in atomic layer deposition process: Density functional theory calculation. Chem Phys 2022;562:111653. https://doi.org/10.1016/j.chemphys.2022.111653.

[13] Han J, Kim Y, Jackson DHK, Jeong KE, Chae HJ, Lee KY, et al. Role of Au-TiO2 interfacial sites in enhancing the electrocatalytic glycerol oxidation performance. Electrochem Commun 2018;96:16–21. https://doi.org/10.1016/j.elecom.2018.09.004.

[14] Wang M, Yang W. Pt nanoparticles Confined in TiO2 Nanotubes With Enhanced Catalytic Performance for Phenol Hydrogenation by Atomic Layer Deposition. Catal Letters 2022;152:1020–8. https://doi.org/10.1007/s10562-021-03702-9.

[15] Chen Y, Wei J, Duyar MS, Ordomsky V V, Khodakov AY, Liu J. Carbon-based catalysts for Fischer-Tropsch synthesis. Chem Soc Rev 2021;5:2337–66. https://doi.org/10.1039/d0cs00905a.

[16] Zhang Q, Cheng K, Kang J, Deng W, Wang Y. Fischer-Tropsch Catalysts for the Production of Hydrocarbon Fuels with High Selectivity. ChemSusChem 2014;7:1251–64. https://doi.org/10.1002/cssc.201300797.

[17] Förtsch D, Pabst K, Groß-Hardt E. The product distribution in Fischer–Tropsch synthesis: An extension of the ASF model to describe common deviations. Chem Eng Sci 2015;138:333–46. https://doi.org/10.1016/J.CES.2015.07.005.

[18] Shahriar MF, Khanal A. The current techno-economic, environmental, policy status and perspectives of sustainable aviation fuel (SAF). Fuel 2022;325. https://doi.org/10.1016/j.fuel.2022.124905.

[19] Eschemann TO, Oenema J, De Jong KP. Effects of noble metal promotion for Co/TiO2 Fischer-Tropsch catalysts. Catal Today 2016;261:60–6. https://doi.org/10.1016/J.CATTOD.2015.06.016.

[20] Sahadat Hossain M, Ahmed S. Easy and green synthesis of TiO2 (Anatase and Rutile): Estimation of crystallite size using Scherrer equation, Williamson-Hall plot, Monshi-Scherrer Model, size-strain plot, Halder- Wagner Model. Results in Materials 2023;20:100492. https://doi.org/10.1016/j.rinma.2023.100492.

[21] National Center for Biotechnology Information. PubChem Compound Summary for CID 26042, Titanium Dioxide 2024.

[22] Yalamaç E, Trapani A, Akkurt S. Sintering and microstructural investigation of gamma–alpha alumina powders. Engineering Science and Technology, an International Journal 2014;17:2–7. https://doi.org/10.1016/j.jestch.2014.02.001.

[23] Reporting physisorption data for gas/solid systems with special reference to the determination of surface area and porosity (Recommendations 1984). Pure and Applied Chemistry 1985. https://doi.org/10.1351/pac198557040603.

[24] Melaet G, Ralston WT, Li CS, Alayoglu S, An K, Musselwhite N, et al. Evidence of highly active cobalt oxide catalyst for the Fischer-Tropsch synthesis and CO2 hydrogenation. J Am Chem Soc 2014;136:2260–3. https://doi.org/10.1021/ja412447q.

# 9. ACRONYMS

- **ALD**: Atomic Layer Deposition
- **BET**: Brunauer-Emmett-Teller
- **CVD**: Chemical Vapor Deposition
- **DEZ**: Diethylzinc
- **FTO**: Fluorine-doped Tin Oxide
- **FTS**: Fischer-Tropsch Synthesis
- **GHG**: Anthropogenic Greenhouse Gas
- **IATA**: International Air Transport Association
- **ICP**: Inductively Coupled Plasma
- **IWI**: Incipient Wetness Impregnation
- **MBE**: Molecular Beam Epitaxy
- **PEC**: Photoelectrochemical
- **PLD**: Pulsed Layer Deposition
- **$SA_{BET}$**: BET Surface Area
- **SAF**: Sustainable Aviation Fuel
- **TDEAT**: Tetrakis(diethylamino)titanium(IV)
- **TDMAT**: Tetrakis(dimethylamino)titanium(IV)
- **TMA**: Trimethylaluminium
- **TPR**: Temperature Programmed Reduction
- **XRD**: X-Ray Diffraction